University of Baghdad
College of Engineering
JE
JOURNAL OF ENGINEERING

Journal of Engineering

journal homepage: www.jcoeng.edu.iq

Volume 31 Number 1 January 2025

Investigating the Moisture Susceptibility Resistance of Asphalt Mixes Modified with Silica Fume Additive

Wasnaa J. Mohammed *, Mohammed Q. Ismael

Department of Civil Engineering, College of Engineering, University of Baghdad, Baghdad, Iraq

ABSTRACT

Moisture induced damage is a prevalent pavement distress commonly observed by road agencies. The damage caused by moisture significantly affects the pavement's lifespan and performance. This research investigated the influence of silica fume (SF) on the susceptibility to moisture. Three concentrations of silica fume were used 3%, 6%, and 9% by weight of the binder. A thermal camera has been used to detect variations in homogeneity in the modified asphalt during the mixing process. The optimal asphalt content was 4.92, 5.02, 5.16, and 5.22 for the control and modified mixtures. The moisture susceptibility was evaluated by measuring the tensile strength ratio (TSR) and index of retained strength (IRS). The thermal images showed that the silica fume particles in the mixture were uniformly distributed, as indicated by the convergence of colors at 160°C. The findings showed that the inclusion of SF at 6% decreased sensitivity to moisture, corresponding to an increase in TSR and IRS of 12.49% and 13%, respectively.

Keywords: Moisture susceptibility, Silica fume, Thermal camera, Indirect tensile strength, Compressive strength.

1. INTRODUCTION

The growth of a country's road network is a crucial measure of its progress **(Mrema and Dida, 2020)**. Most people agree that highways significantly influence societal, economic, and social advancement **(Abtahi et al., 2010)**. One of the elements that contribute to pavement deterioration prematurely is moisture sensitivity **(Klinsky et al., 2018)**. Moisture infiltration into the asphaltic pavement is a significant problem that leads to stripping, fatigue cracking, raveling, bleeding, and permanent deformation **(Nazal and Ismael, 2019)**. When water is present at the interface of asphalt concrete pavement, the bonding force between the different parts of asphalt and aggregate degrades, causing the binder to be stripped from the surface of the aggregate (loss of adhesion) and the cohesive failure of the

*Corresponding author
Peer review under the responsibility of University of Baghdad.
https://doi.org/10.31026/j.eng.2025.01.05

Article received: 28/05/2024
Article revised: 12/08/2024
Article accepted: 19/08/2024
Article published: 01/01/2025

asphalt binder itself (loss of cohesion) **(Behiry, 2013; Das et al., 2015; Kakar et al., 2015).** Moisture susceptibility is recognized as the primary performance issue that affects the durability of asphalt pavements. The presence of moisture in asphalt pavement causes a decrease in its stiffness and structural integrity. Researchers have employed various test methods to assess moisture susceptibility, such as indirect tensile strength and compressive strength. These tests compare the strength or stiffness of the specimens before and after their exposure to moisture **(Do et al., 2019)**. In order to prevent the degradation of mixtures, moisture susceptibility must be properly assessed **(Vargas-Nordcbeck et al., 2016).** Pavement's performance, durability, and service life are mostly depend on the amount of bitumen that can attach and bind to the aggregate surface under various circumstances **(Omar et al., 2020).** Hence, the most effective and prevalent method for raising the asphalt mixture's resistance to moisture is to employ anti-stripping additives **(Hamedi and Tahami, 2018)**. The key goal of including anti-stripping substances is to enhance the binding between the aggregate and binder while keeping good HMA characteristics, thus decreasing the sensitivity of the asphalt mixture to moisture **(Sebaaly, 2007; Al-Saad and Ismael, 2022).**

Silica fume (SF) is a residual substance generated during the smelting process employed for the production of silicon and ferrosilicon alloys, which involves reducing high-purity quartz with coal in electric furnaces. Almost 90% of the components of SF are usually made up of minuscule amorphous silicon dioxide (SiO_2) particles found in the material. Other names for SF include condensed SF, volatilized silica, micro silica, and silica dust **(Khodary, 2016; Siddique and Mehta, 2020; Zheng et al., 2020; Albeer and Hassan, 2023).**

(SF) has been identified as a pozzolanic additive. Its size is less than 100–150 times that of cement **(Fattouh et al., 2023)**. According to previous investigations, adding SF to asphalt binder raises the softening point, increases viscosity, and decreases penetration **(Akpolat et al., 2022).** Researchers have used a variety of additives in order to improve the asphalt mixture's performance and lessen its sensitivity to moisture**(Ismael et al., 2023).** Generally, the inclusion of additives increases stiffness, enhances temperature sensitivity, and decreases moisture sensitivity **(Haider et al., 2020).** To introduce modifiers into pavement construction, researchers have incorporated a variety of additives into the ordinary binder, such as fly ash, silica fumes, sulfur, hydrated lime, and nanomaterials **(Sarsam and Lafta, 2014; Jasim and Ismael, 2021).**

Three percents (1.0%, 1.5%, and 2.0%) of hydrated lime were added by **(Ismael and Ahmed, 2019)** to modify the asphalt mixes' susceptibility to moisture. The results showed a higher increase in resistance to moisture damage for AC (40–50) and AC (60–70) grades.

(Taher and Ismael, 2022) showed the effects of adding nanosilica (NS) at concentrations of 2%, 4%, and 6% to asphalt on (HMA) mixtures' susceptibility to moisture under various aging conditions, revealing that the NS improves pavement performance by improving volumetric characteristics and stability while lowering susceptibility to moisture damage**.**

(Al-Taher et al., 2018) utilized silica fume at percentages of 2%, 4%, 6%, and 8% by weight of bitumen, according to their findings that the Marshall stability, indirect tensile strength rose by around 23.61%, 3.83%, respectively, at a silica fume percentage of 6%. **(Naser et al., 2023)** revealed that asphalt mixtures including silica fume showed significant behavior concerning stability, The highest increase was recorded at a 75% silica fume addition, SF was utilized as a filler with steel slag at four different percents by weight of the aggregate: 25%, 50%, 75%, and 100%**.** The bitumen weight contents of an asphalt mixture including binders modified with silica fume at 3%, 5%, 7%, and 10% were evaluated by **(Shafabakhsh**

et al., 2015). Their results showed that, in contrast to normal asphalt, silica fume improved the creep behavior of HMA at high temperatures and stress levels.
The major objective of this research is to evaluate the impact of silica fume on the moisture susceptibility of the wearing course of the improved asphalt mixture in comparison to a control mixture (i.e the original mixture without any additive).

2. MATERIALS

All materials used are compatible with the criteria of the Iraqi Specification for Roads and Bridges **(SCRB/R9, 2003)** and are readily accessible locally.

2.1 Asphalt Cement

This work utilized an asphalt binder (40–50) penetration class, which was obtained from Al-Durrah Refinery in Baghdad. **Table 1.** displays the physical characteristics of the asphalt cement used in this study. **Table 2.** presents some of the physical characteristics of the modified asphalt with SF

Table 1. Asphalt cement characteristics.

Test	Unit	Results	SCRB	Standard ASTM
Penetration (25°C, 100 g, and 5 sec)	0.1 mm	44	40 - 50	**(ASTM D5, 2013)**
Softening point (Ring & Ball)	°C	52	-----	**(ASTM D36, 2014)**
Specific Gravity, at 25°C	----	1.045	-----	**(ASTM D70, 2012)**
Ductility@ 25°C, 5 cm/min	cm	162	≥ 100	**(ASTM D113, 2007)**
Flash point(Cleveland open Cup)	°C	276	>232	**(ASTM D92, 2012)**
After the Film Oven Test				**(ASTM D1754, 2009)**
Retained Penetration, of original	%	62	>55	**(ASTM D5, 2013)**
Retained Ductility@ 25°C	cm	76	>25	**(ASTM D113, 2007)**

Table 2. Some of the Physical characteristics of asphalt modified with SF.

Test	Unit	Results		
		SF 3%	SF 6%	SF 9%
Penetration (25°C, 100 g, and 5 sec)	0.1 mm	39	35	28
Softening point (Ring & Ball)	°C	54	55	60
Ductility@ 25°C, 5 cm/min	cm	158	147	133

2.2 Aggregate

The Al-Nibaai quarry's fine and coarse aggregate was used. The coarse aggregate, for the wearing course ranged in sieve diameters from 3/4 in (19 mm) to No. 4 (4.75 mm), while the fine aggregate size was observed to vary between No. 4 (4.75 mm) and No. 200 (0.075 mm) sieve. **Table 3.** provides various physical characteristics of both fine and coarse aggregate. The asphalt mixture's aggregate grade was chosen to satisfy Iraqi requirements for the surface or wearing course Type IIIA **(SCRB/R9, 2003)**. **Fig. 1** displays the gradation of aggregate.

Table 3. Physical characteristics of Coarse and fine aggregate.

Property	Standard ASTM	Result	SCRB
Coarse Aggregate			
Bulk Specific Gravity	**(ASTMC127,2015)**	2.58	-----
Water Absorption %	**(ASTMC127,2015)**	0.55	-----
Los Angeles Abrasion %	**(ASTM C131, 2020)**	16	30 max
Fine Aggregate			
Bulk Specific Gravity	**(ASTM C128, 2015)**	2.61	-----
Water Absorption %	**(ASTM C128, 2015)**	0.81	-----

2.3 Mineral Filler

In this investigation, the asphalt mixture was made with limestone dust because it was available and inexpensive. The filler, which is provided from the Iraqi lime factory in Karbala, is sieved through an opening of 0.075 mm. The **(SCRB/R9, 2003)** requirement was followed in selecting the filler shown in **Table 4**.

Table 4. Characteristics of limestone dust

Property	Result	SCRB Requirement
% Passing Sieve No.200	95	70-100
Specific Gravity	2.69	-----

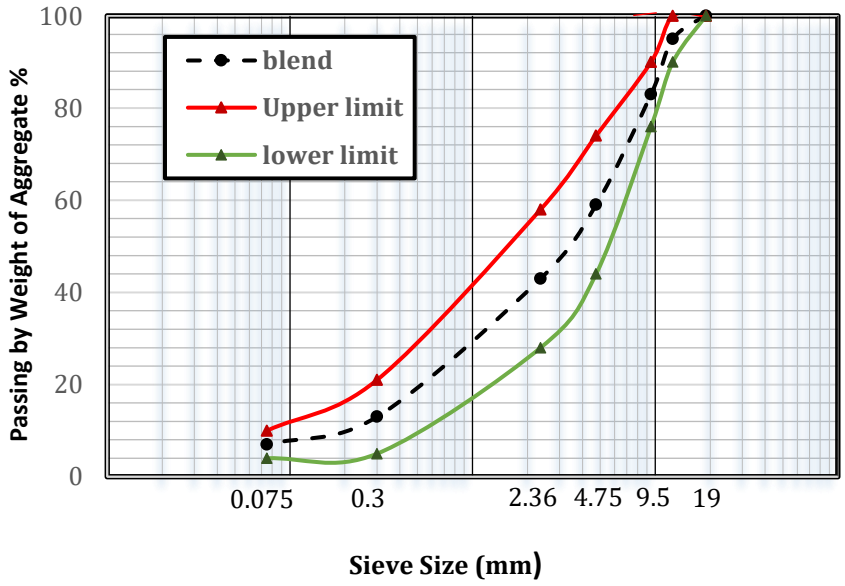

Figure 1. The gradation of aggregate (by researcher based on **(SCRB/R9, 2003)**).

2.4 Silica Fume (SF)

SF was added to asphalt mixes as a binder modifier to enhance their performance and reduce their susceptibility to moisture by 3, 6, and 9% of the binder weight. SF is by product of the manufacture of elemental silicon or silicon-containing alloys in electric arc furnaces, superfine non-crystalline silicon dioxide (SiO_2) particles. **Fig. 2** illustrates the SF

used in this work, while **Table 5.** exhibits the chemical characteristics of SF based on the X-ray fluorescence test results. **Table 6.** displays the physical characteristics of SF based on the product technical document.

Figure 2. Photo of silica fume.

Table 5. Chemical characteristics of silica fume.

SiO_2 %	SO_3%	CaO%	Fe_2O_3 %	Al_2O_3 %	LOI
94.5	0.11	2.04	0.37	0.11	Max 6%

Table 6. Physical characteristics of silica fume.

Appearance	Bulk Density kg/m^3	Surface Area m^2/g	Specific Gravity	retained on sieve 45 micron
Gray to medium gray	(500-700)	Min 15	(2.10-2.40)	Max 10%

2.5 Blending Silica Fume (SF) with Asphalt

In order to effectively carry out the blending of SF with asphalt cement, various devices including a thermal camera, tachometer, and mixer were employed, as illustrated below:

2.5.1 Compact Thermal Imager (Thermal Camera)

The UTi120P thermal imager was utilized in this study. Thermal imagers convert invisible infrared rays into visible thermal images. The accuracy of a thermal camera primarily depends on emissivity, which is defined as the ability of an object for reflecting the temperature of its surface by the infrared radiation emitted from it **(Albatici et al., 2013)**. For this camera, the emissivity was determined for various materials, including concrete, asphalt, black aluminum, water, bricks, and copper. The emissivity value for asphalt was found to be 0.96. In other words, if the emissivity were equal to 1, then the infrared rays emitted by the material, when measured by the thermal camera (infrared sensor), would accurately represent the real temperature with 100% accuracy. **Table 7** exhibits the characteristics of thermal camera and images.

2.5.2 Digital Laser Tachometer Instrument

The digital tachometer instrument has been used to measure the rotation speed in revolutions per minute of a shaft or disk in a motor or any rotary device. A laser tachometer emits a laser beam. The beam is aimed at a reflective strip (tape) on the

rotating object. The laser spot should be visible on the reflective tape. These strips were attached to the rotating part of a mechanical mixer for reflecting the tachometer instrument's laser signal, allowing for accurate signal receipt from the moving section. When the light beam makes contact with this tape, it is then redirected back towards the light sensor located in the tachometer. The device will record the frequency of occurrences when the reflected signal is received. Consequently, the reading was expressed in rotations per minute. In this study, the mixer reached 1500 rpm, as shown in **Fig. 3.**

Table 7. Characteristics of thermal camera and images.

Technical data	Uti 120p
IR resolution (pixels)	120*90
Thermal sensivity	≤ 60 mk
Temperature range	-20 °C~400 °C
Accuracy	± 2°C
Emissivity	0.01 ~ 0.99 adjustable
Response time	≤ 500 ms
Image mode	Thermal
Color palettes	3 (iron bow, grey, rainbow)
Image format	Bitmap (BMP)

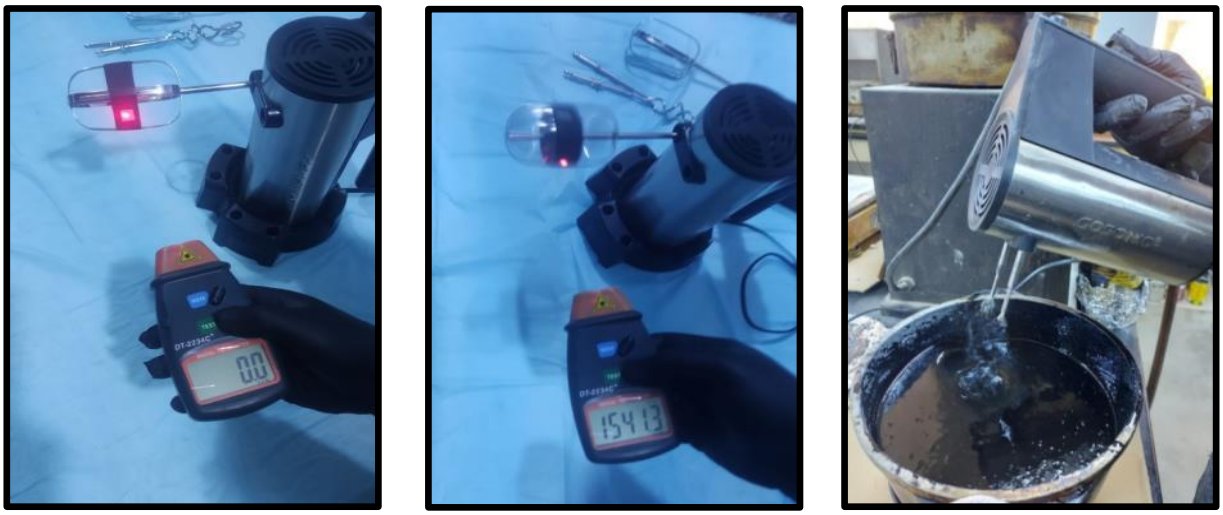

(a)Before turning on the mixer (b) Device at 1500 rpm (c) Blending SF with asphalt

Figure 3. Tachometer device and mixer.

2.5.3 Trail Method of Mixing Silica Fume with Asphalt

A trial method was employed to determine the appropriate mixing temperature. The necessary uniformity was monitored through the utilization of a thermal imaging device. Three temperatures were used (150,160, and 170°C) **(Sarsam and AL-Lamy, 2015; Zheng et al., 2020; Akpolat et al., 2022)** at 1500 rpm that was measured previously. The images showed that the homogeneity of asphalt containing silica fume appears after 45 minutes at 150°C, while it occurs after 30 minutes at 160°C. At 170°C, homogeneity happens

after 30 minutes, but bubbles were noticed. Consequently, 160°C was selected as the most suitable temperature for achieving the necessary homogeneity in a short time. It will be explained later through thermal analysis. Thermal images illustrating the steps of mixing using a thermal camera are shown in **Figs. 4 to 8.** Three different concentrations of SF (3%, 6%, and 9% by weight of the binder) were added to asphalt cement to modify it. To complete the mixing procedure, a mechanical mixer was used to modify the asphalt with SF. SF was added gradually to the asphalt after it had heated to 160°C, and the mixer was running at 500 rpm to ensure that the SF particles were evenly dispersed. After 5 minutes, the speed of mixing was increased to 1500 rpm for (30 minutes) as a constant blending time **(Alhamali et al., 2016; Ezzat et al., 2016).**

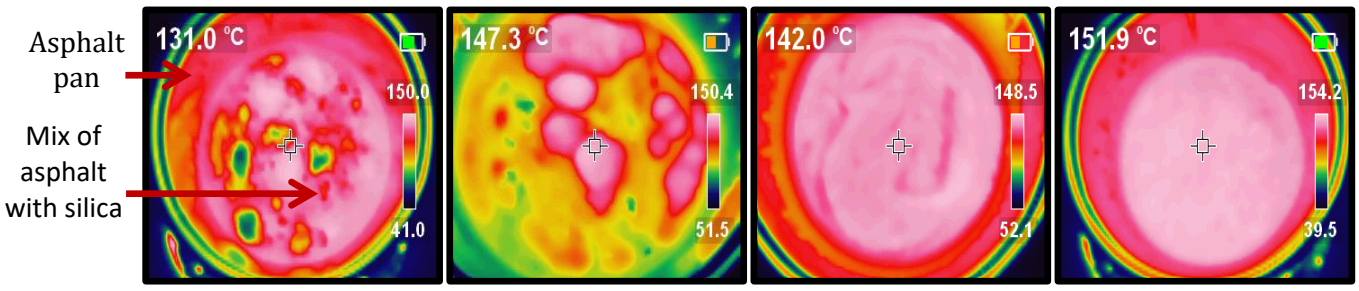

(a) After (0.5) min. (b) After (5) min. (c) After (15) min. (d) After (45) min.

Figure 4. Thermal images of mixing 6% silica fume with asphalt at 150°C.

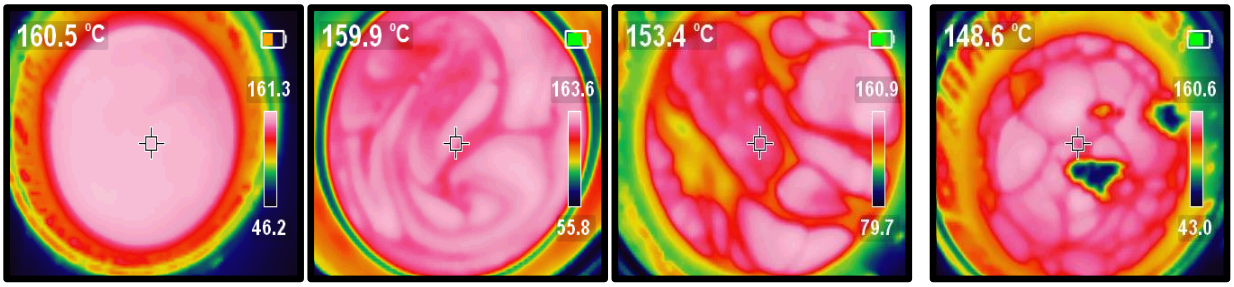

(a) After (0.5) min. (b) After (5) min. (c) After (15) min. (d) After (30) min.

Figure 5. Thermal images of mixing 6% silica fume with asphalt at 160°C.

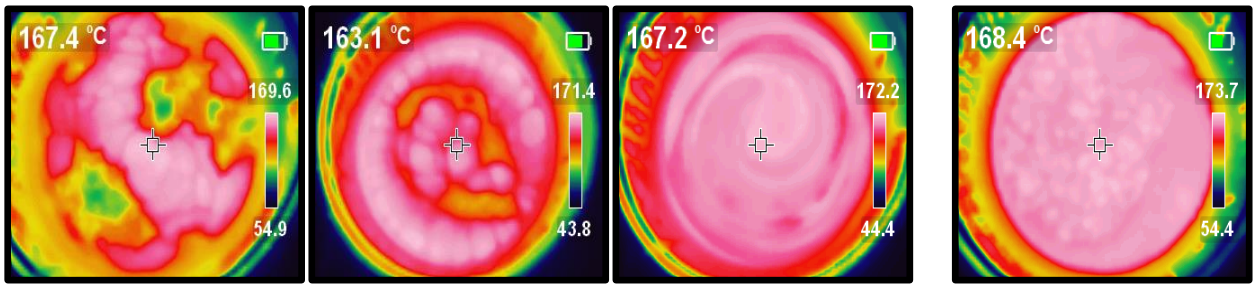

(a) After (0.5) min. (b) After (5) min. (c) After (15) min. (d) After (30) min.

Figure 6. Thermal images of mixing 6% silica fume with asphalt at 170°

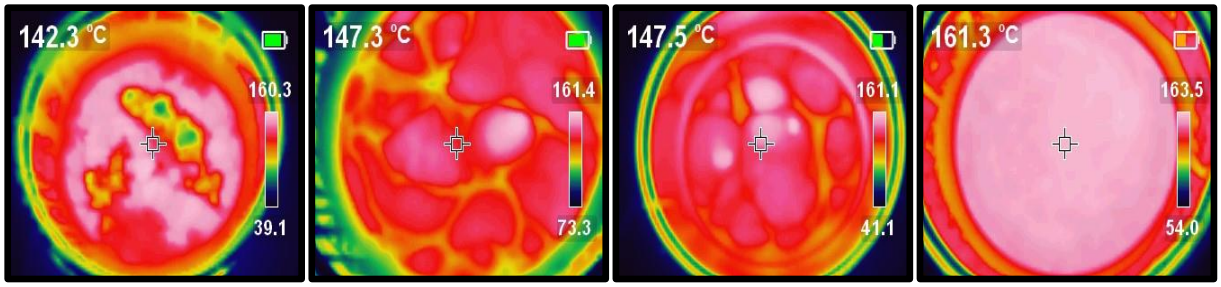

(a) After (0.5) min. (b) After (5) min. (c) After (15) min. (d) After (30) min.

Figure 7. Thermal images of mixing 3% silica fume with asphalt at 160°C.

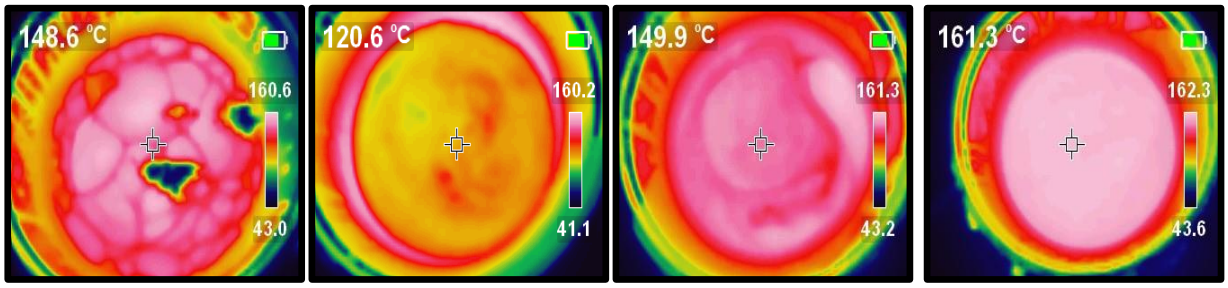

(a) After (0.5) min. (b) After (5) min. (c) After (15) min. (d) After (30) min.

Figure 8. Thermal images of mixing 9 % silica fume with asphalt at 160°C.

3. EXPERIMENTAL WORK

Firstly, the Marshall approach has been used to determine the O.A.C. for the conventional mixture and each percentage of silica fume additive. To assess the asphalt mixture's resistance to moisture degradation, the index of retained strength and the tensile strength ratio were calculated. Compressive strength and indirect tensile testing were utilized to find these parameters.

3.1 Marshall Test

The O.A.C. for the chosen aggregate gradation was determined using the Marshall mix design method. Three specimens were created for each of the asphalt contents (4-6%), utilizing (12.5mm) nominal maximum size aggregate in every mixture. After the mold had been compacted, it was moved on a flat surface and allow cool down at ambient temperature for 20 hours until it was removed. For the control mix and each percentage of the silica fume addition, identical samples with measurements of 63.5 mm in height and 101.6 mm in diameter were created. Next, following **(ASTM D6927, 2015)**, the specimens were prepared for testing by immersing them in a water bath at 60°C for 30 minutes. Lastly, take the specimen out of the water bath and use a towel to wipe off any remaining water. Then, immediately put it into the Marshall Apparatus and note the stability and flow values. In this design approach, the Asphalt Institute's recommended O.A.C. was determined by selecting 4% of air voids as the primary factor. All other characteristics, such as bulk density, flow,

Marshall stability, and voids, were evaluated in the criteria in order to ascertain the required specifications, and this process has been repeated for other mixes modified with SF with different concentrations of 3%, 6%, and 9% by weight of the binder**(Islam, 2020)**. **Table 8.** is a summary of the O.A.C results. **Fig. 9** shows the specimens and Marshall test, and **Fig. 10** displays the Marshall characteristics for the control mixture.

Table 8. The outcomes of Marshall test

O.A.C. (%)	Stability (kN)	Flow (mm)	Bulk density (gm/cm^3)	A.V. (%)	V.M.A (%)	V.F.A (%)
4.92	9.89	3.28	2.333	4	14.71	72.80
SCRB (R9) for wearing coarse						
4-6	Min 8	2-4	___	3-5	Min 14	___

Figure 9. The specimens and Marshall test.

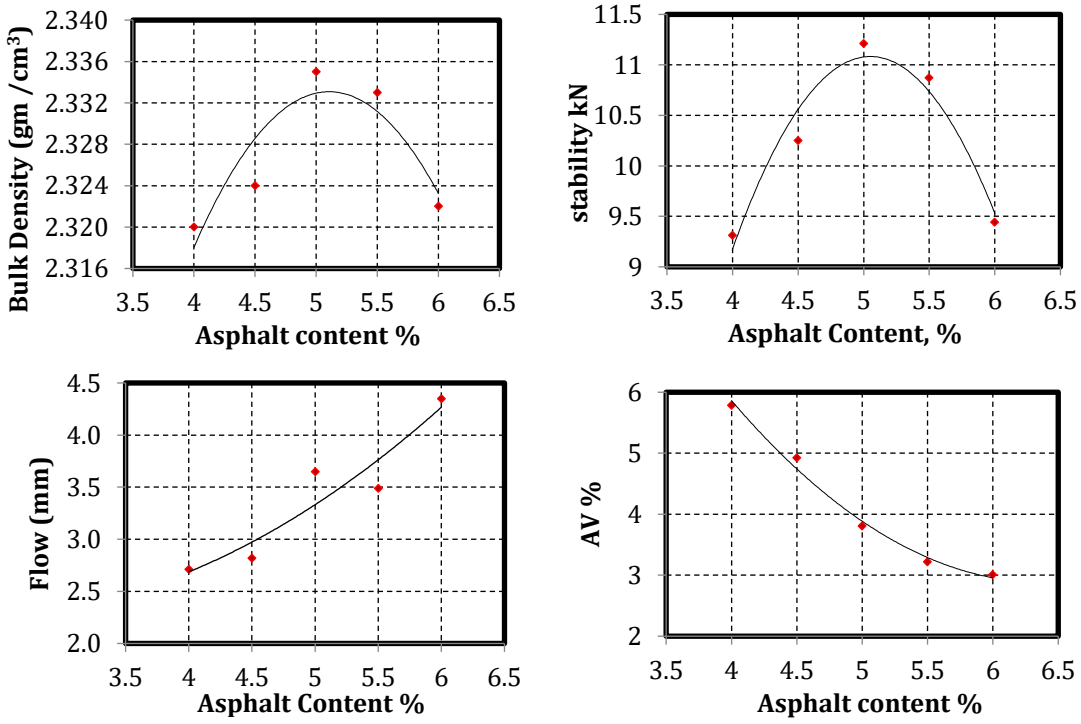

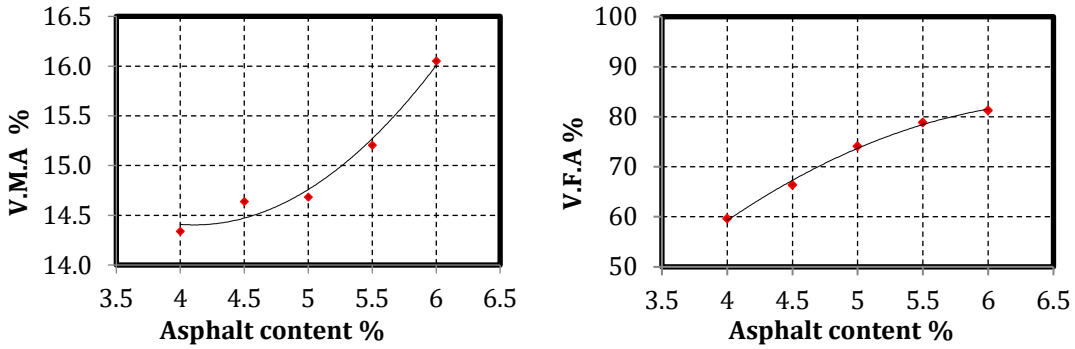

Figure 10. Marshall characteristics for the control mixture.

3.2 Indirect Tensile Strength

The moisture sensitivity of the asphalt mixture was assessed using the ASTM D4867. The calculation of the number of blows required to generate 7% ±1 air spaces is shown in **Fig. 11**

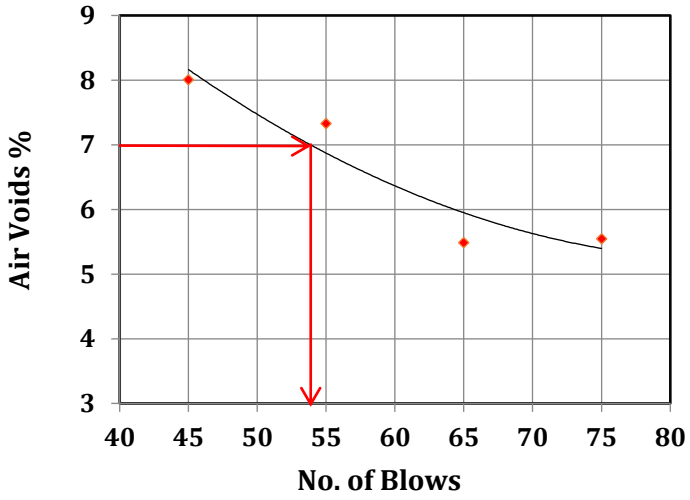

Figure 11. Correlation between the number of blows and the percent of air voids.

After calculating the blows, four groups were created from the Marshall samples, each consisting of two sets, each set including three samples. There was no additive in one of the groups, while the other groups received modifications consisting of 3%, 6%, and 9% of SF. The initial set of samples was chosen as unconditioned samples. These samples were submerged in a water bath at 25°C for a duration of 30 minutes. Subsequently, they were subjected to an (ITS) test. The second set of samples from every group was placed in water at temperature 25°C while being exposed to a vacuum in order to exclude air. After that, the samples were treated to one cycle of freezing and thawing, which involved being frozen for 16 hours at -18°C and then thawed for 24 hours at 60°C. Then, the specimens were extracted and immersed in a water bath at temperature 25°C for aduration of one hour, repeating the identical test with the initial set. **Fig. 12.** illustrates the test's procedure. The ITS and TSR value were calculated using the following Eq. (1) , Eq. (2)

$$ITS\% = \frac{2000\ Pult.}{\pi\ tD} * 100 \quad (1)$$

$$TSR\% = \frac{ITS\ con}{ITS\ uncon} * 100 \quad (2)$$

Where:-
- ITS : indirect tensile strength (kPa)
- *P ult.:* The ultimate load failure (N),
- *D*: sample's diameter (mm).
- *t:* sample's height (mm).
- ITScon. : indirect tensile strength of wet samples
- ITSuncon. : indirect tesile strength of dry samples

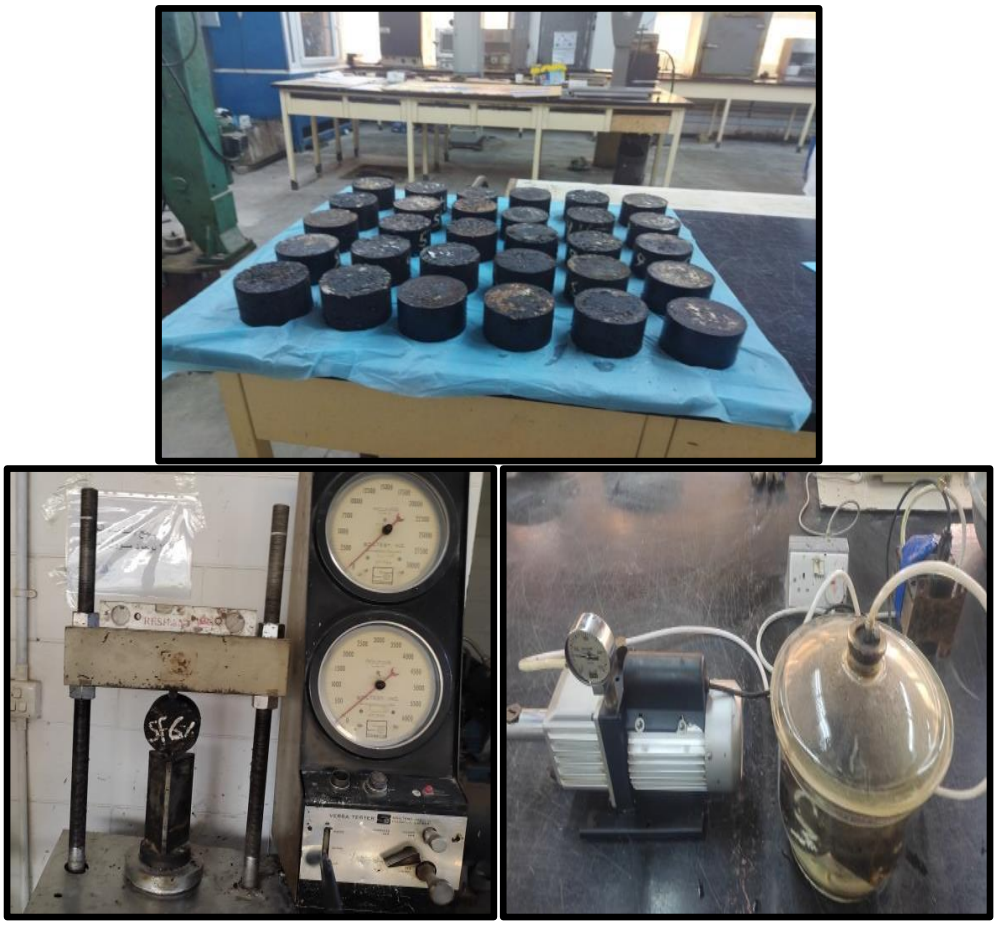

Figure 12. The indirect tensile strength test.

3.3 Compressive Strength Test

The index of retained strength (IRS) was employed to assess the resistance of a mixture to moisture degradation. The lowest allowable value of (IRS) is 70%, according **(SCRB/R9, 2003)**. This test was conducted in compliance with **(ASTM D1074, 2011).** The asphalt mixture was compressed utilizing a compressed device until the specimen achieves the appropriate height (4 inch). The specimen has a height and diameter of 4 inch (101.6 x 101.6 mm) **(Mawat and Ismael, 2020; Abdi Kordani et al., 2021)**. The specimens were chilled

for a whole day, prior to experiencing a loading rate of 5.08 mm/min during the compressive strength test. After that, the specimens were placed vertically such that the initial surface of the specimen could be subjected to axial force until it failed as explained in **(ASTM1075, 2011). Fig. 13** shows the test specimens for compressive strength.

$$IRS = \frac{S2}{S1} * 100 \quad (3)$$

Where,
S1: The compressive strength of the dry sample (kPa);
S2: The compressive strength of immersed sample (kPa)

Figure 13. Compressive strength samples

4. RESULTS AND DISCUSSION

4.1 Thermal Analysis

The thermal analysis software linked to the thermal camera was employed to evaluate the uniformity of surface temperatures of asphalt enhanced with silica fume, as illustrated in the thermal image analysis presented in **Figs. 14 to 18.**
The primary substance depicted in these images consists of a blend of asphalt and silica fume. Through thermal analysis, fluctuations in temperature are observed during the various stages of mixing, ultimately revealing the achievement of the intended uniformity over the course of the process.
In all the images, in (a) and (b), it was found that there is a mixture of colors ranging from low to high, but as mixing continues, homogeneity occurs, as illustrated in (c) and (d).
Homogeneity can be observed through the convergence of temperatures recorded at various points and for different colors through thermal analysis until a significant convergence in temperatures and colors is achieved, indicating their suitability for the mixing process. Therefore, 160 degrees was chosen due to the similarity in temperature at most points on the surface.

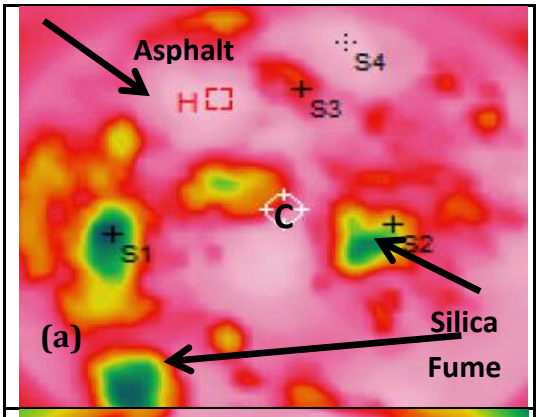

Center temperature (C)		131°C	
High (H) temperature		150°C	
S1	S2	S3	S4
68°C	93.8°C	118.2°C	148.7 °C

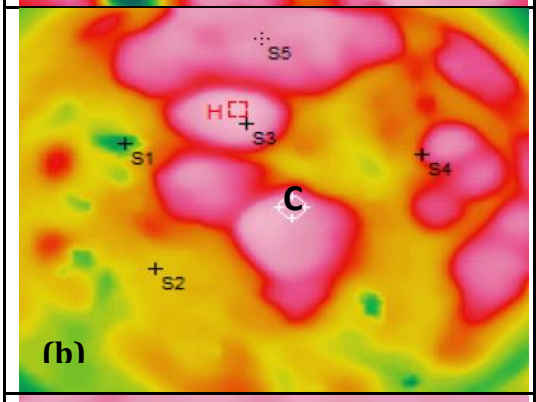

Center temperature(C)		147.3°C		
High (H) temperature		150.4°C		
S1	S2	S3	S4	S5
86°C	101.3°C	147°C	125 °C	140 °C

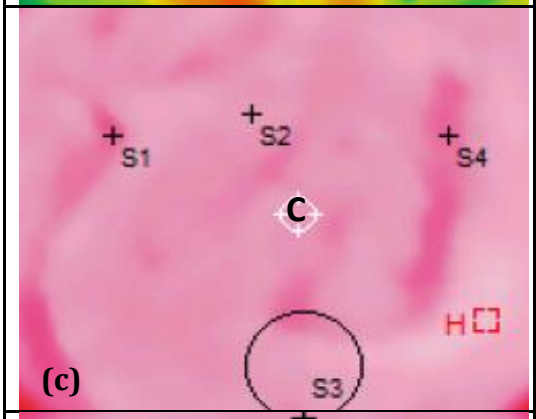

Center temperature (C)		142°C	
High (H) temperature		149°C	
S1	S2	S3	S4
133.7°C	141.3°C	145.1°C	134.8 °C

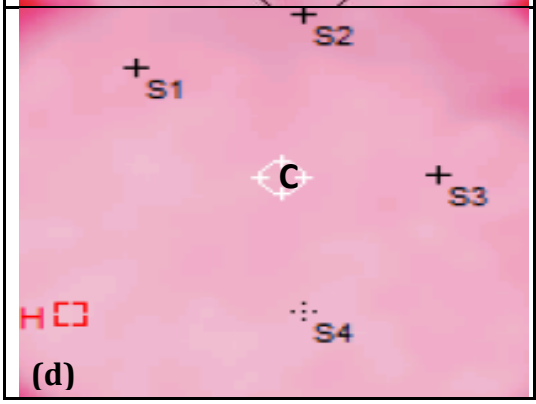

Center temperature(C)		151.9°C	
High (H) temperature		154.2°C	
S1	S2	S3	S4
149.7°C	143.8°C	150.1°C	152.4 °C

Figure 14. Thermal analysis to images of mixing 6% SF with asphalt at 150°C.

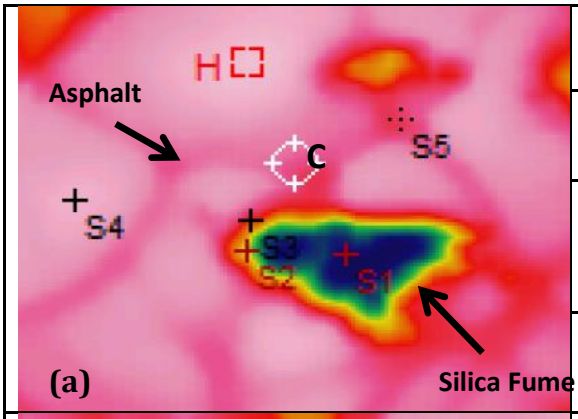

Center temperature(C)		148.6°C			
High (H) temperature		160.6°C			
S1	S2	S3	S4	S5	
60°C	100.4°C	126°C	157.4°C	135.1°C	

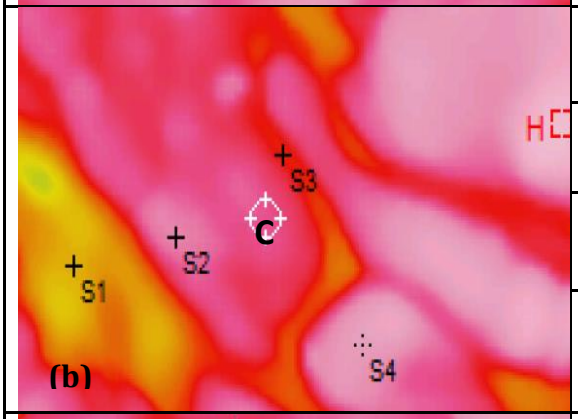

Center temperature(C)		153.4°C	
High (H) temperature		160.9°C	
S1	S2	S3	S4
122.5°C	151.6°C	136.9°C	155.1°C

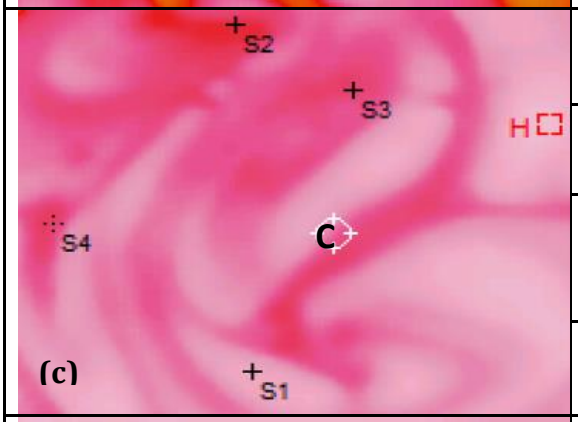

Center temperature(C)		159.9°C	
High (H) temperature		163.6°C	
S1	S2	S3	S4
158.5°C	136.9°C	142.4°C	142°C

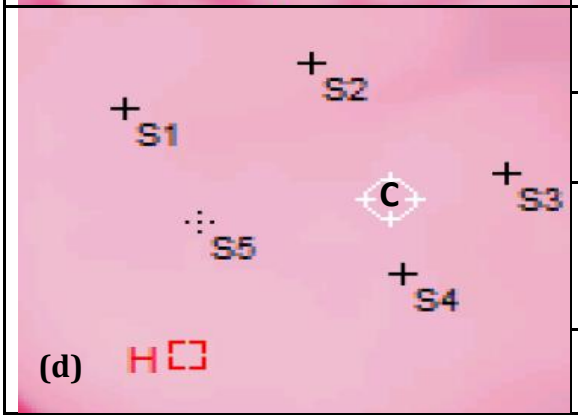

Center temperature(C)		160.5°C		
High (H) temperature		161.3°C		
S1	S2	S3	S4	S4
159.9°C	159.9°C	159°C	159.9°C	159°C

Figure 15. Thermal analysis to images of mixing 6% SF with asphalt at 160°C.

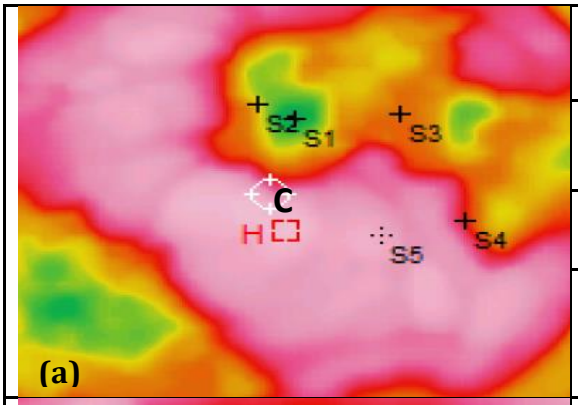

Center temperature(C)		167.4 ℃			
High (H) temperature		169.9℃			
S1	S2	S3	S4	S4	
94.6℃	111.8℃	126℃	137℃	164℃	

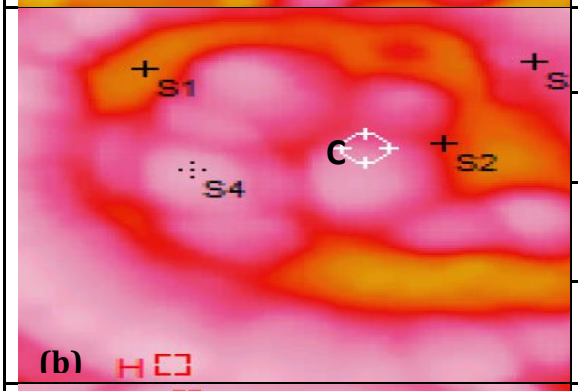

Center temperature(C)		163.1 ℃	
High (H) temperature		171.4 ℃	
S1	S2	S3	S4
120.7℃	133.2℃	149.3℃	163.9℃

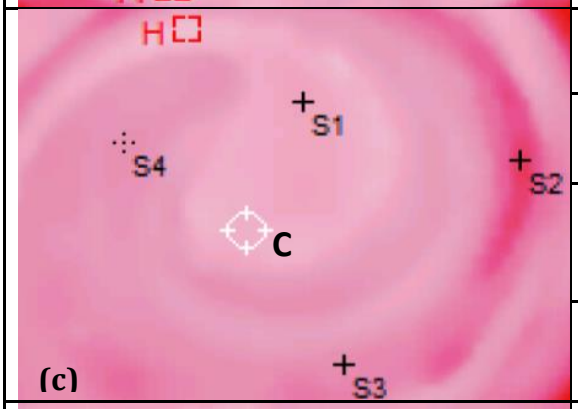

Center temperature(C)		167.2 ℃	
High (H) temperature		172.2℃	
S1	S2	S3	S4
165.7℃	145℃	158.6℃	159.1℃

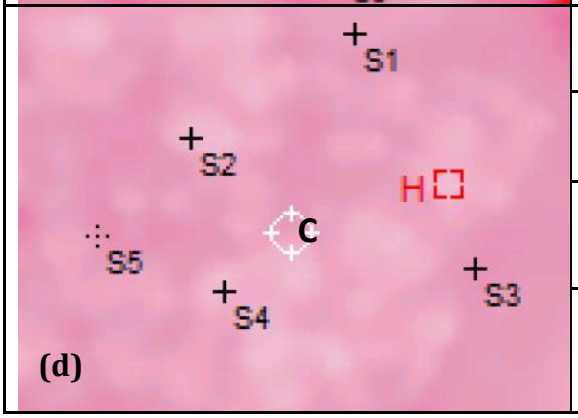

Center temperature(C)		168.4 ℃		
High (H) temperature		173℃		
S1	S2	S3	S4	S5
166.7℃	172.3℃	163℃	171.8 ℃	163℃

Figure 16. Thermal analysis to images of mixing 6% SF with asphalt at 170℃.

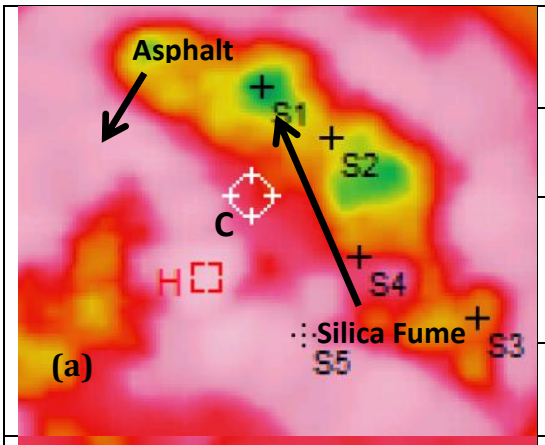

Center Temperature (C)		142.3°C			
High (H) Temperature		160.3°C			
S1	S2	S3	S4	S5	
77.8°C	99.2°C	113.1 °C	126.4 °C	151.7°C	

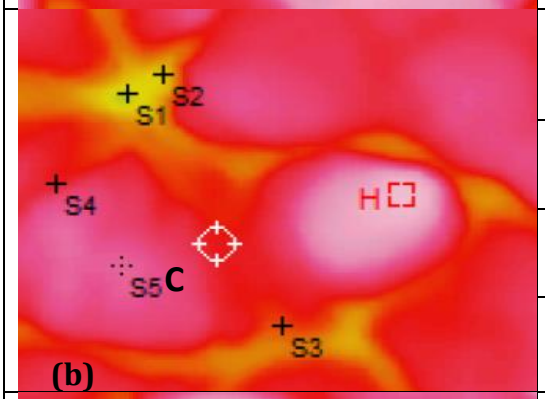

Center Temperature(C)		147.3°C		
High (H) Temperature		161.4°C		
S1	S2	S3	S4	S5
114°C	118°C	131.6 °C	138°C	148.6 °C

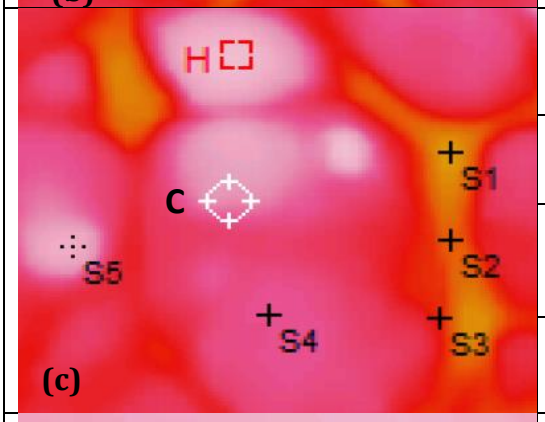

Center Temperature (C)		147.5°C		
High (H) Temperature		161.1°C		
S1	S2	S3	S4	S5
108.7°C	118°C	124°C	141°C	156°C

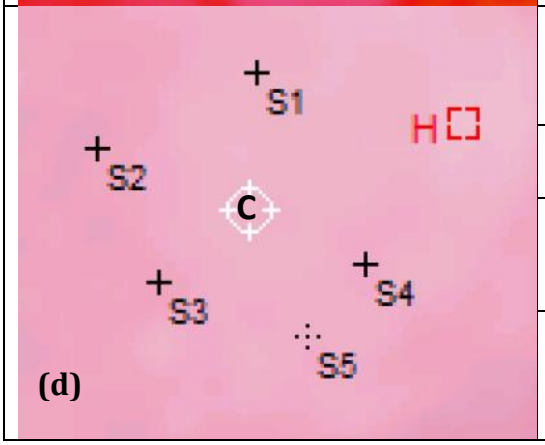

Center Temperature(C)		161.3°C		
High (H) Temperature		163.5°C		
S1	S2	S3	S4	S5
161°C	159°C	158°C	159°C	160°C

Figure 17. Thermal analysis to images of mixing 3% SF with asphalt at 160°C.

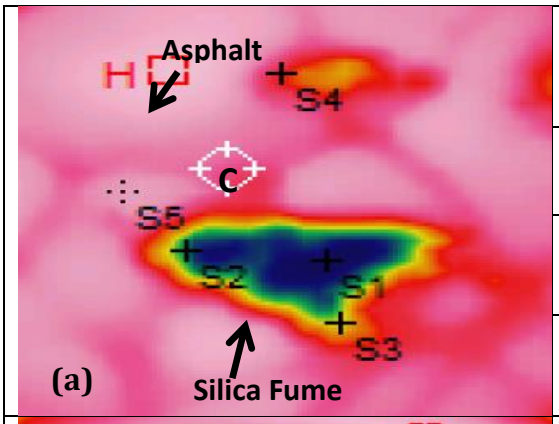

Center Temperature (C)		148.6°C			
High (H) Temperature		160.6°C			
S1	S2	S3	S4	S5	
57.8°C	75.9°C	101 °C	128°C	151.8°C	

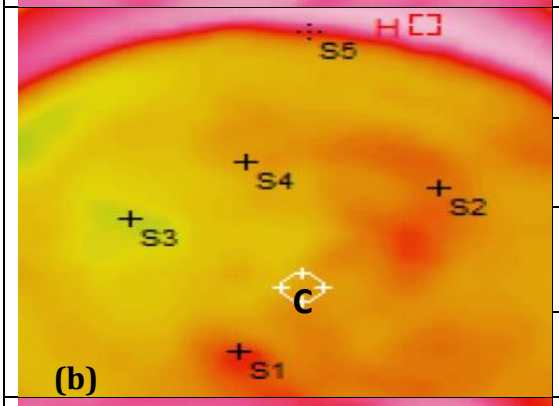

Center Temperature(C)		120.6°C		
High (H) Temperature		160.2°C		
S1	S2	S3	S4	S5
122°C	114.2°C	96.4 °C	107°C	129°C

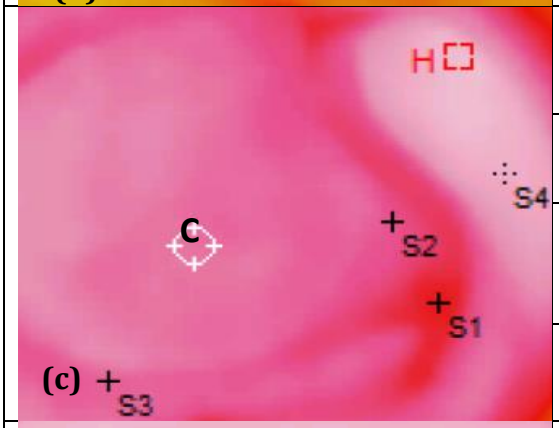

Center Temperature (C)		149.9°C	
High (H) Temperature		161.3°C	
S1	S2	S3	S4
128.8°C	141.8°C	143.6°C	156.7°C

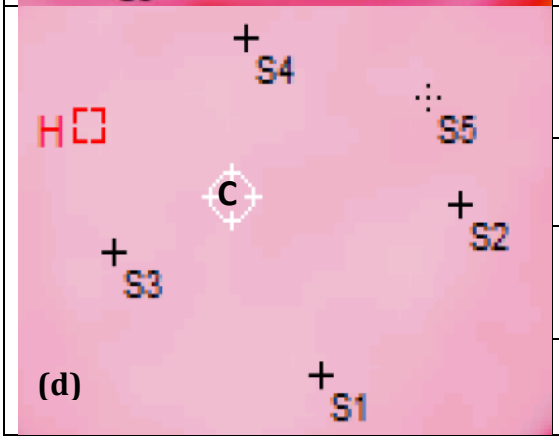

Center Temperature(C)				161.3°C	
High (H) Temperature				162.3°C	
S1	S2	S3	S4	S5	S6
160.9 °C	161 °C	161 °C	160 °C	160.4°C	159.5°C

Figure 18. Thermal analysis to images of mixing 9% SF with asphalt at 160°C.

4.2 Marshall Test

With the inclusion of 3%, 6%, and 9% of SF, the (O.A.C) rose from 4.92% in original binder to 5.02%, 5.16%, and 5.22% in an enhanced binder. According to the Marshall stability results, as seen in **Fig. 19**. adding 3, 6, and 9% SF raised the mixture's Marshall stability by (12.43, 20.42, and 15.36%) respectively. The highest stability increase was obtained at 6% silica fume. The findings demonstrated that, despite an increase in asphalt composition, the Marshall flow dropped by 5.79 and 14% with the addition of 3 and 6% of SF, respectively. When the SF concentration reached 9%, the flow started to climb again, although it was still dropping in comparison to the control mix, which had a 3.13 mm decline of 4.57%. **Fig. 20.** displays that the effect of SF on the Marshall flow. Because of the increased surface area of SF, there is a rise in binder stiffness, which contributes to this enhancement in stability and leads to a drop in flow. As the percentage of SF rose to 9%, the bulk density increased. The mixture got denser as a result of the large surface area of SF applied to the binder. **Fig. 21.** demonstrates how SF affects the asphalt mixture's density, while keeping the air voids percentage (AV%) within the permitted limits. As to the **(SCRB/R9, 2003)**, 3-5% of AV is sufficient to avoid bleeding that results from asphalt with low AV (below 3%) mixture. However, a high AV (above 5%) reduces the resistance of asphalt mixture to fatigue and moisture. As seen in **Fig. 22.** the inclusion of 3%, 6%, and 9% of SF resulted in a drop in the VMA%. The high surface area of the SF resulted in a greater number of voids being filled with bitumen. This, in turn, enhanced the ability of the asphalt to fill the voids and create a more durable asphalt mixture, as demonstrated by **Fig. 23.** A drop in voids in mineral aggregate percentage may be linked with the rise in density. **Table 9.** presents the collected test results of the impact of SF. These outcomes are in agreement with **(Shafabakhsh et al., 2015; Zheng et al., 2020; Zhu and Xu, 2021)**.

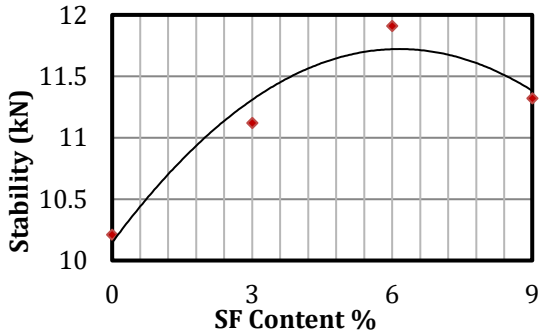

Figure 19. Impact of SF on Marshall stability.

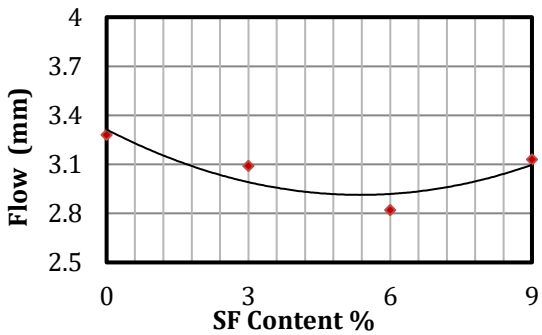

Figure 20. Impact of SF on Marshall flow.

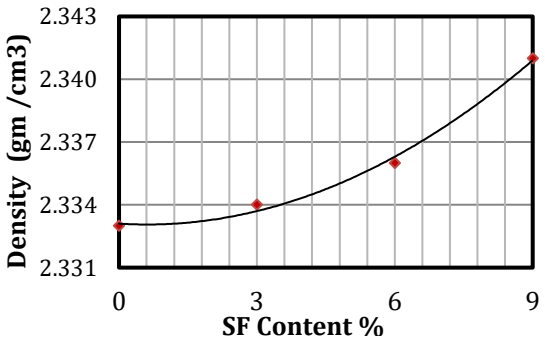

Figure 21. Impact of SF on bulk density.

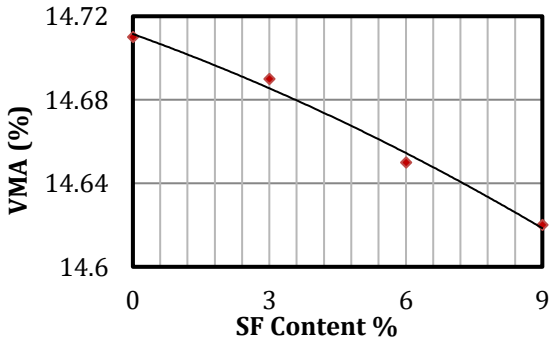

Figure 22. Impact of SF on VMA.

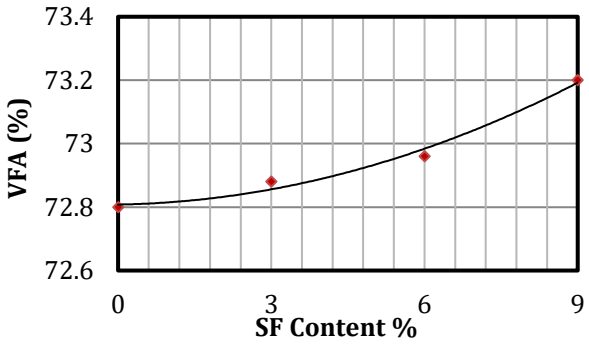

Figure 23. Impact of SF on VFA.

Table 9. Impact of Silica Fume on Marshall characteristics.

S.F (%)	O.A.C. (%)	Stability (kN)	Bulk density (gm/cm^3)	Flow (mm)	AirVoids (%)	V.M.A (%)	V.F.A (%)
0	4.92	9.89	2.333	3.28	4	14.71	72.80
3	5.02	11.12	2.334	3.09	4	14.69	72.88
6	5.16	11.91	2.336	2.82	4	14.65	72.96
9	5.22	11.41	2.341	3.13	4	14.62	73.20

4.3 Tensile Strength Ratio

The inclusion of SF by weight of binder enhanced both the wet and dry tensile strength. Consequently, T.S.R values rose, with the tensile strength ratio having the most growth at 6% SF percent. In comparison to the control mix, TSR value rose by 12.49%. as a result of increase bonding between binder and aggregate due to high surface area and cementation effect of SF. The results also indicated that there was a convergence between the TSR values for the control mix and 3% SF, which may be attributed to the ratio being insufficient enough to increase adhesion between the components of the asphalt mix. **Table 10.** As well as **Fig. 24** display each of the data required for the test. The results align with the research conducted by **(Al-Taher et al., 2018; Al-Ani, 2020).**

Table 10. Tensile strength ratio outcomes.

SF (%)	Dry I.T.S (kPa)	Wet I.T.S (kPa)	T.S.R (%)
0	1227	1008	82.12
3	1386	1167	84.22
6	1467	1355	92.38
9	1397	1223	87.54

4.4 Index of Retained Strength

In this test, the index of retained strength (IRS) was employed to assess the compressive strength of the asphalt mix while exposed to water. Similar to the tensile strength ratio's growing trend, adding 3%, 6%, 9% of Silica Fume additive enhances both wet and dry of compressive strength values. Therefore, the amount of the (IRS) also enhanced by 6% as a best acquired findings. The highest obtained in (IRS) value over the control mixture was 13%, and this resulted in a decrease in the asphalt mixture's sensitivity to moisture, where moisture resistance increased as IRS increased. The test results are summarized in **Table 11**. As well as are illustrated in **Fig. 25.** The findings are compatible with **(Al-Taher et al., 2018).**

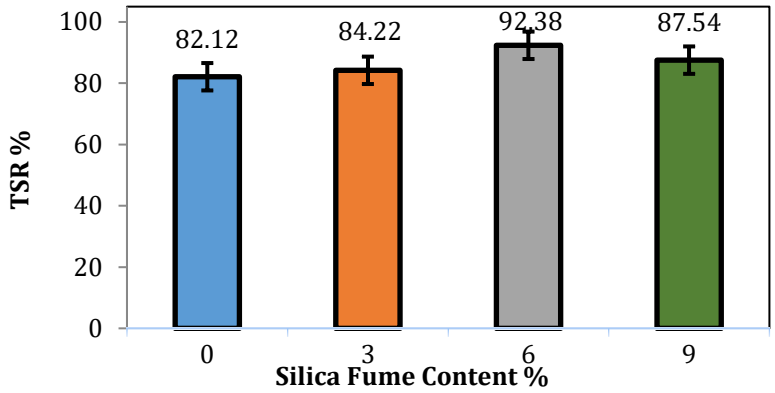

Figure 24. Impact of silica fume on TSR.

Table 11. Index of retained strength findings.

SF (%)	Dry Compressive Strength (kPa)	Wet Compressive Strength (kPa)	I.R.S (%)
0	8658	6543	75.56
3	10418	8511	81.69
6	11889	10159	85.45
9	11293	8874	78.58

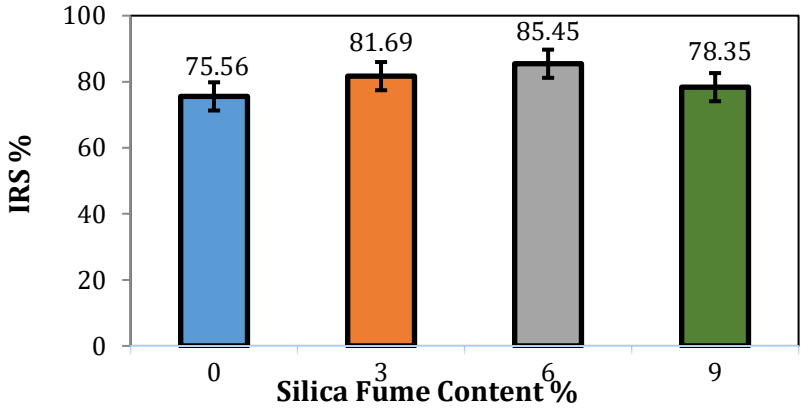

Figure 25. Impact of Silica Fume on IRS.

5. CONCLUSIONS

This study investigates the effectiveness of asphalt mixtures containing silica fume on moisture susceptibility. The resistance of the asphalt mix to moisture was assessed by the utilization of indirect tensile strength and compressive strength tests. The results led to the following conclusions:

- The tensile strength ratio (TSR) values rise with the inclusion of SF by weight of binder, indicating a reduction in the asphalt mixture's sensitivity to moisture. The inclusion of 6% SF produced the greatest TSR of 92.38%, compared to the control mixture's 82.12% TSR. This led to a 12.49% increase in the (TSR).
- The inclusion of 6% of SF also led to the highest IRS, which was 85.45% compared to the 75.56% control mixture. With this amount, the (IRS) was raised by 13%.
- The thermal images revealed a consistent distribution of SF particles in the asphalt cement through the homogeneity of colors following 30 min. of blending SF at 160 °C.

- The incorporation of SF with three percents (3, 6, and 9%) of the binder's weight enhanced the Marshall characteristics of the asphalt mixes. The inclusion of 6% SF resulted in the highest Marshall stability, measuring 11.91 kN, whereas the control mixture recorded 9.89 kN. The Marshall stability was increased by 20.42% with this amount.
- Marshall flow dropped with the addition of SF; the largest decrease in Marshall flow was 14% when 6% of SF was added, whereas the air voids percentage (AV%) remained within permitted limits.
- The best SF content for increasing TSR and IRS and reducing moisture sensitivity was 6% when mixed with asphalt at 160 °C for 30 minutes using a 40/50 asphalt cement.

NOMENCLATURE

Symbol	Description	Symbol	Description
HMA	Hot Mix Asphalt	SCRB	State Corporation for Roads and Bridges
SF	Silica Fume	ASTM	American Society for Testing and Material
VFA	Voids Filled with Asphalt	ITS	Indirect Tensile Strength
VMA	Voids Mineral Aggregate	IRS	Index of Retained Strength
AV	Air Voids	D	sample's diameter, mm
O.A.C.	Optimal Asphalt Content	TSR	Tensile Strength Ratio
P	The ultimate load failure	t	Sample's height, mm

Acknowledgments

In conducting the experimental work for this research, the Transportation Laboratory of the University of Baghdad's Civil Engineering Department provided significant help, for which the authors are grateful.

Credit Authorship Contribution Statement

Wasnaa J. Mohammed: writing the initial version, editing it, preparing the experimental part, materials, and analysing the outcomes. Mohammed Q. Ismael: writing, revising, edting, supervising, developing techniques, and Validation.

Declaration of Competing Interest

The authors declare that they have no known competing financial interests or personal relationships that could have appeared to influence the work reported in this paper.

REFERENCES

Abdi Kordani, A., Seifi, S.H., Ghasemzadeh Tehrani, H. and Shirini, B., 2021. The effect of different deicing solutions on the moisture susceptibility of asphalt mixture. *SN Applied Sciences*, 3, pp.1–14. https://link.springer.com/article/10.1007/s42452-021-04613-5.

Abtahi, S.M., Sheikhzadeh, M. and Hejazi, S.M., 2010. Fiber-reinforced asphalt-concrete–a review. *Construction and Building Materials*, 24(6), pp.871–877. https://doi.org/10.1016/j.conbuildmat.2009.11.009.

Akpolat, M., Kök, B.V. and Aydoğmuş, E., 2022a. Research on the rheological properties of asphalt binder modified by fume silica and crumb rubber compound. *Periodica Polytechnica Civil Engineering*, 66(2), pp.502–515. https://doi.org/10.3311/PPci.19139.

Al-Ani, A.F., 2020. The impact of utilizing silica fume as a filler on asphalt concrete mixes. *Key Engineering Materials*, 857, pp.22–31. https://doi.org/10.4028/www.scientific.net/ KEM. 857 .22.

Al-Saad, A.A. and Ismael, M.Q., 2022. Rutting prediction of hot mix asphalt mixtures reinforced by ceramic fibers. *Journal of Applied Engineering Science*, 20(4), pp.1345–1354. http://doi:10.5937/jaes0-38956.

Al-Taher, M.G., Hassanin, H.D., Ibrahim, M.F. and Sawan, A.M., 2018. Investigation of the effect of adding silica fume on asphalt concrete properties. *International Journal of Engineering Research*, 7(4), pp.48–55. https://doi.org/10.5958/2319-6890.2018.00095.8.

Albatici, R., Passerini, F., Tonelli, A.M. and Gialanella, S., 2013. Assessment of the thermal emissivity value of building materials using an infrared thermovision technique emissometer. *Energy and buildings*, 66, pp.33–40. https://doi.org/10.1016/j.enbuild.2013.07.004.

Albeer, S.J. and Hassan, M.S., 2023. Silica fume modified cement-based mortar exposed to high temperatures: residual strengths and microstructure. *Journal of Engineering*, 29(7), pp.18–33. https://doi.org/10.31026/j.eng.2023.07.02.

Alhamali, D.I., Wu, J., Liu, Q., Hassan, N.A., Yusoff, N.I.M. and Ali, S.I.A., 2016. Physical and rheological characteristics of polymer modified bitumen with nanosilica particles. *Arabian Journal for Science and Engineering*, 41, pp.1521–1530. https://doi.org/10.1007/s13369-015-1964-7.

Anon. 2016. Effect of Lime Addition Methods on Performance Related Properties of Asphalt Concrete Mixture. *Journal of Engineering*, [online] 22(9 SE-Articles), pp.1–20. https://doi.org/10.31026/j.eng.2016.09.01.

ASTM 1075, 2011. Standard test method for effect of water on compressive strength of compacted bituminous mixtures. http://doi: 10.1520/D1075-07.

ASTM D92, 2012. *Standard test method for flash and fire points by Cleveland open cup tester*. ASTM International. http://doi:10.1520/D0092-12A.

ASTM D6927, 2015 standard test method for Marshall stability and flow of asphalt mixtures. *ASTM International: West Conshohocken, PA, USA*. http://doi:10.1520/D6927-15.

ASTM 127, 2015. Standard test method for relative density (specific gravity) and absorption of coarse aggregate. *ASTM West Conshohocken, PA*. http://doi:10.1520/C0127-15.

ASTM D113, 2007. Standard test method for ductility of bituminous materials. ASTM West Conshohocken, PA. http://doi:10.1520/D0113-07.

ASTM D1754, 2009. Standard test method for effects of heat and air on asphaltic materials (thin-film oven test). *Annual book of ASTM standards*, http://doi: 10.1520/D1754_D1754M-09R14.

ASTM D5, 2013. Standard test method for penetration of bituminous materials. *USA, ASTM International*. http://doi: 10.1520/D0005-06.

ASTM C131/C131M, 2020. Standard Test Method for Resistance to Degradation of large-Size Coarse Aggregate by Abrasion and Impact in the Los Angeles Machine, ASTM International, West Conshohocken, PA. i, pp.1–2. http://doi: 10.1520/C0131_C0131M-20.

ASTM D36, 2014. Standard test method for softening point of bitumen (ring-andball apparatus). *American Association of State and Highway Transportation Officials, Washington, DC*. http://doi: 10.1520/D0036_D0036M-12.

Behiry, A.M., 2013. Laboratory evaluation of resistance to moisture damage in asphalt mixtures. *Ain Shams Engineering Journal*, 4(3), pp.351–363. https://doi.org/10.1016/j.asej.2012.10.009.

Das, P.K., Baaj, H., Kringos, N. and Tighe, S., 2015. Coupling of oxidative ageing and moisture damage in asphalt mixtures. *Road Materials and Pavement Design*, 16(sup1), pp.265–279. https://www.tandfonline.com/doi/abs/10.1080/14680629.2015.1030835.

Do, T.C., Tran, V.P., Lee, H.J. and Kim, W.J., 2019. Mechanical characteristics of tensile strength ratio method compared to other parameters used for moisture susceptibility evaluation of asphalt mixtures. *Journal of Traffic and Transportation Engineering (English Edition)*, 6(6), pp.621–630. http://dx.doi.org/10.1016/j.jtte.2018.01.009.

Ezzat, H., El-Badawy, S., Gabr, A., Zaki, E.-S.I. and Breakah, T., 2016. Evaluation of asphalt binders modified with nanoclay and nanosilica. *Procedia engineering*, 143, pp.1260–1267. https://doi.org/10.1016/j.proeng.2016.06.119.

Fattouh, M.S., Tayeh, B.A., Agwa, I.S. and Elsayed, E.K., 2023. Improvement in the flexural behaviour of road pavement slab concrete containing steel fibre and silica fume. *Case Studies in Construction Materials*, 18, p.e01720. https://doi.org/10.1016/j.cscm.2022.e01720.

Haider, S., Hafeez, I., Zaidi, S.B.A., Nasir, M.A. and Rizwan, M., 2020. A pure case study on moisture sensitivity assessment using tests on both loose and compacted asphalt mixture. *Construction and Building Materials*, 239, p.117817. https://doi.org/10.1016/j.conbuildmat.2019.117817.

Islam, M.R., 2020. Asphalt mix design. *Civil Engineering Materials*, https://doi.org/10.1201/9780429275111-7.

Ismael, M.Q. and Ahmed, A.H., 2019b. Effect of hydrated lime on moisture susceptibility of asphalt mixtures. *Journal of Engineering*, https://doi.org/10.31026/j.eng.2019.03.08.

Ismael, M.Q., Joni, H.H. and Fattah, M.Y., 2023. Neural network modeling of rutting performance for sustainable asphalt mixtures modified by industrial waste alumina. *Ain Shams Engineering Journal*, 14(5), p.101972. https://doi.org/10.1016/j.asej.2022.101972.

Jasim, S.A. and Ismael, M.Q., 2021. Marshall performance and volumetric properties of styrene-butadiene-styrene modified asphalt mixtures. *Civil Engineering Journal*, 7(6), pp.1050–1059. http://dx.doi.org/10.28991/cej-2021-03091709.

Kakar, M.R., Hamzah, M.O. and Valentin, J., 2015. A review on moisture damages of hot and warm mix asphalt and related investigations. *Journal of Cleaner Production*, 99, pp.39–58. https://doi.org/10.1016/j.jclepro.2015.03.028.

Khodary, F., 2016. Impact of Silica fume on the properties of Asphalt pavement base course. *Civil Engineering Department, Qena Faculty of Engineering, South Valley University, Qena, Egypt, International Journal of Engineering Trends and Technology (IJETT)*. https://doi.org/10.14445/22315381/IJETT-V35P297.

Klinsky, L.M.G., Kaloush, K.E., Faria, V.C. and Bardini, V.S.S., 2018. Performance characteristics of fiber modified hot mix asphalt. *Construction and Building Materials*, *176*, pp.747-752. https://doi.org/10.1016/j.conbuildmat.2018.04.221.

Mawat, H.Q. and Ismael, M.Q., 2020. Assessment of moisture susceptibility for asphalt mixtures modified by carbon fibers. *Civil Engineering Journal*, 6(2), pp.304–317. https://doi.org/10.28991/cej-2020-03091472.

Mrema, I.J. and Dida, M.A., 2020. A survey of road accident reporting and driver's behavior awareness systems: The case of Tanzania. *Engineering, Technology & Applied Science Research*, 10(4), pp.6009–6015. https://doi.org/10.48084/etasr.3449.

Naser, M., Abdel-Jaber, M., Al-Shamayleh, R., Ibrahim, R., Louzi, N. and AlKhrissat, T., 2023. Improving the mechanical properties of recycled asphalt pavement mixtures using steel slag and silica fume as a filler. *Buildings*, 13(1), 132. https://doi.org/10.3390/buildings13010132.

Nazal, H.H. and Ismael, M.Q., 2019. Evaluation the moisture susceptibility of asphalt mixtures containing demolished concrete waste materials. *Civil Engineering Journal*, 5(4), pp.845–855. http://dx.doi.org/10.28991/cej-2019-03091293.

Omar, H.A., Yusoff, N.I.M., Mubaraki, M. and Ceylan, H., 2020. Effects of moisture damage on asphalt mixtures. *Journal of Traffic and Transportation Engineering (English Edition)*, 7(5), pp.600–628. https://doi.org/10.1016/j.jtte.2020.07.001.

Sarsam, S.I. and AL-Lamy, A.K., 2015. Fatigue life assessment of modified asphalt concrete. *International Journal of Scientific Research in Knowledge*, 3(2), p.30. http://dx.doi.org/10.12983/ijsrk-2015-p0030-0041.

Sarsam, S.I. and Lafta, I.M., 2014. Assessment of modified-asphalt cement properties. *Journal of Engineering*, 20(06), pp.1–14. https://doi.org/10.31026/j.eng.2014.06.01.

SCRB/R9, 2003. *General Specification for Roads and Bridges, Section R/9, Hot-Mix Asphalt Concrete Pavement, Revised Edition*. *State Corporation of Roads and Bridges, Ministry of Housing and Construction, Republic of Iraq*.

Sebaaly, P.E., 2007. *Comparison of lime and liquid additives on the moisture damage of hot mix asphalt*. https://doi.org/11714/4926.

Shafabakhsh, G., Ani, O.J. and Mirabdolazimi, S., 2015. Experimental investigation on rutting performance of microsilica modified asphalt mixtures. *International Journal of Engineering Research & Technology (IJERT)*, 4, pp.371–378. https://doi.org/10.1016/j.conbuildmat.2015.08.083.

Siddique, R. and Mehta, A., 2020. Utilization of industrial by-products and natural ashes in mortar and concrete development of sustainable construction materials. In: *Nonconventional and vernacular construction materials*. Elsevier. pp.247–303. https://doi.org/10.1016/B978-0-08-100038-0.00007-X.

Taher, Z.K. and Ismael, M.Q., 2022. Rutting prediction of hot mix asphalt mixtures modified by nano silica and subjected to aging process. *Civil Engineering Journal*, 9, pp.1–14. https://doi.org/10.28991/CEJ-SP2023-09-01.

Vargas-Nordcbeck, A., Leiva-Villacorta, F., Aguiar-Moya, J.P. and Loria-Salazar, L., 2016. Evaluating moisture susceptibility of asphalt concrete mixtures through simple performance tests. *Transportation Research Record*, 2575(1), pp.70–78. https://doi.org/10.3141/2575-08.

Zheng, X., Xu, W., Feng, H. and Cao, K., 2020. High and low temperature performance and fatigue properties of silica fume/SBS compound modified asphalt. *Materials*, 13(19), p.4446. https://doi.org/10.3390/ma13194446.

Zhu, J. and Xu, W., 2021. Aging resistance of silica fume/styrene-butadiene-styrene composite-modified asphalt. *Materials*, 14(21), p.6536. https://doi.org/10.3390/ma14216536.

التحقق من تحسس الرطوبة للخلطات الإسفلتية المعدلة بمضاف غبرة السيليكا

وسناء جاسم محمد*، محمد قادر اسماعيل

قسم الهندسة المدنية، كلية الهندسة، جامعة بغداد، بغداد، العراق

الخلاصة

يعد الضرر الناتج عن الرطوبة من مشاكل التبليط الخطيرة التي تواجهها معظم منظمات الطرق. بالإضافة إلى ذلك، يؤثر الضرر الناتج عن الرطوبة بشكل كبير على عمر الرصيف وأدائه. يهدف هذا البحث إلى دراسة تأثير غبرة السيليكا على حساسية الخلطات الإسفلتية للرطوبة. تم استخدام ثلاثة تراكيز من مادة غبرة السيليكا المضافة 3%، 6% و9% كنسبة من وزن السمنت الاسفلتي. تم استخدام كاميرا حرارية للتعرف على تغيرات التجانس في الأسفلت المعدل اثناء عملية الخلط. وكان المحتوى الاسفلتي الأمثل 4.92 ،5.02،5.16،5.22 للخلطة الاساسية والخلطات المحسنة. حدد هذا البحث نسبة الشد غير المباشر (TSR)، ومؤشر القوة المتبقية (IRS) لتقييم قابلية الرطوبة. وفقا للصور الحرارية كانت جزيئات غبرة السيليكا موزعة بشكل منتظم في الاسفلت من خلال تقارب الالوان عند درجة حرارة 160 درجة سيليزية. أظهرت النتائج ان إدراج غبرة السيليكا بنسبة 6٪ ادى إلى تقليل الحساسية للرطوبة، بما يتوافق مع زيادة في نسبة الشد غير المباشر (TSR) ومؤشر القوة المتبقية (IRS) وبنسب 12.49%و13% على التوالي.

الكلمات المفتاحية: تحسس الرطوبة، غبرة السيليكا، الكاميرا الحرارية، مقاومة الشد غير المباشر، مقاومة الانضغاط.